Molecular Science

AIMS Molecular Science, 3(4): 661-682.
DOI: 10.3934/molsci.2016.4.661
Received 9 September 2016,
Accepted 6 November 2016,
Published 14 November 2016

http://www.aimspress.com/journal/Molecular

Research article

A proteomic analysis of the interactions between poly(L-lactic acid) nanofibers and SH-SY5Y neuronal-like cells

Ana Marote[1,†], Nathalie Barroca[2,†], Rui Vitorino[1,3], Raquel M. Silva[1,4], Maria H.V. Fernandes[2], Paula M. Vilarinho[2], Odete A.B. da Cruz e Silva[1], and Sandra I. Vieira[1,*]

[1] iBIMED—Institute for Biomedicine, Department of Medical Sciences, Universidade de Aveiro, 3810-193 Aveiro, Portugal
[2] CICECO—Centre for Research in Ceramics and Composite Materials, Department of Materials and Ceramic Engineering, Universidade de Aveiro, 3810-193 Aveiro, Portugal
[3] QOPNA—Organic Chemistry, Natural Products and Food Stuffs, QOPNA, Universidade de Aveiro, 3810-193 Aveiro, Portugal
[4] iEETA—Institute of Electronics and Informatics Engineering of Aveiro, Universidade de Aveiro, 3810-193 Aveiro, Portugal

† Both authors contributed equally to this work.

* **Correspondence:** E-mail: sivieira@ua.pt; Tel: (+351) 234247256; Fax: (+351) 234372587.

Abstract: Poly (L-lactic acid) (PLLA) is a biodegradable and biocompatible polymer that has been put forward as a promising material for therapeutic approaches aiming to restore neuronal function. The topographic cues present in PLLA-based scaffolds, defined by the technique used in their preparation, have been shown to play a role on the cellular behavior of adherent cells. Even though this interaction has been shown to influence the regenerative output of the scaffold, there is a lack of studies addressing this response at the proteomic level. Hence, this work focuses on the effect of electrospun PLLA-based nanofibers on the proteome, cellular processes and signaling pathways of SH-SY5Y neuroblastoma cells. It also further explores how these molecular mediators might influence cell proliferation and differentiation upon in vitro culture. For that, mass spectrometry followed by bioinformatics analysis was firstly performed and further complemented with Western blot, cell viability and imaging assays. Results show that PLLA nanofibers differentially activate and inhibit specific cellular functions and signaling pathways related to cell division, apoptosis, actin remodeling, among others. These ultimately block cellular proliferation and induce morphological rearrangements through cytoskeleton remodeling, adaptations that turn cells more prone to

differentiate. In synthesis, PLLA nanofibers shift the SH-SY5Y cells proteome towards a state more responsive to differentiation-inductive cues such as the retinoic acid. Unveiling cells responses to nanomaterials is an important step to increase the tools available for their manipulation and potentiate their use in neural tissue engineering. Further studies should be performed to compare the effects of other topographic cues on cellular behavior.

Keywords: poly (L-lactic) acid scaffolds; nanofibers; cellular adaptation to nanomaterials; neuroregeneration; signaling for neuronal differentiation

1. Introduction

The development of scaffolds that provide cues to induce faster tissue regeneration is a major field of tissue engineering. Biodegradable scaffolds based on materials such as polyglycolic acid, type-I collagen, and poly(85:15/L:D) lactide-ε-caprolactone have been used for nerve regeneration purposes [1-3]. These platforms aim to improve adhesion, proliferation and differentiation of neuronal precursor cells and neurons, and may include chemical and physical cues that optimize those processes. Neurons can improve their differentiation by responding to electric and topographical features present in their microenvironment. Nanofibrous scaffolds have been observed to help neuronal differentiation as neurites grow along the nanofibers meshes [2-7]. Electrical stimuli have also been shown to improve neuronal development and function [1,3,8-10], and can be delivered by piezoelectric materials. These have the ability to produce electricity in response to mechanical stress, in the absence of any external energy supply. Nanofibers-based platforms prepared from piezoelectric materials are thus promising nanomaterials for neuroregeneration [2,7,4,11,12]. Examples of nanofibrous piezoelectric scaffolds used to enhance cellular neuritogenesis include scaffolds based on annealed polyvinylidene fluoride-trifluoroethylene (PVDF-TrFE). These can enhance neuritic extension in dorsal root ganglion [13] and promote differentiation of human neural progenitor cells [14]. However, PVDF is a non-degradable polymer.

Poly (L-lactic) acid (PLLA) is a FDA-approved synthetic piezoelectric polymer that possesses significant advantages over other piezoelectric materials tested for neural repair so far, including its biodegradability. PLLA, as other helical polymers like polypeptides, generates shear piezoelectricity depending on the mechanical orientation of its macromolecules in the crystalline and quasi-crystalline regions. It can further present tensile piezoelectricity and a controllable polarization after an appropriate electrical poling that induces the orientation of the dipoles in its molecules [15]. In bone, the PLLA piezoelectric character can induce electric fields that stimulate osteocytes activity and accelerate bone repair [16]. The biocompatibility and biodegradability of PLLA enhance its potential for neural tissue engineering, as observed both *in vitro* [4-7,11,12,17,18] and *in vivo* [19]. In 2005, Yang and colleagues reported the first electrospun aligned PLLA scaffold for neural application, showing that neural stem cells differentiate when cultured on these PLLA nanofibrous scaffolds [4,11]. Thenceforward, several papers have explored the ability of PLLA nanofibers to promote neuritic outgrowth [4,3,6,10,17], and our group has proven that electrical polarization of PLLA nanofibers further enhances their neuritogenic effect (unpublished data).

Regardless, the molecular and cellular alterations induced by the PLLA nanofibrous platforms to their target cells are far from clarified. At the cellular level, electrical stimulation and the

nanofibers' topology can initiate molecular signaling for cellular adhesion, neuroprotection, and cytoskeleton remodeling processes. These are crucial in neuronal regeneration to *de novo* activate specific genes and stimulate local protein synthesis leading to structural remodeling of the injured neuron required, e.g., to form new growth cones [9]. The interaction of neuronal cells with PLLA electrospun nanofibers was recently evaluated [20]. These authors have used the human neuroblastoma SH-SY5Y cell line, a widely used in vitro model of neuronal differentiation [21], and unraveled a role for integrin and increased pERK in the PLLA nanofibers-SH-SY5Y cell interaction [20]. In this study, we aimed to further evaluate SH-SY5Y cellular processes and molecular pathways altered in response to PLLA nanofibers through a high-throughput proteomic analysis. Major cellular processes and signaling pathways influenced by the exposure of SH-SY5Y cells to the PLLA nanofibrous platforms were thus analyzed by mass spectrometry. These were related to cell viability and morphology, and to protein levels of key molecules. Our results show alterations of the cellular proteome towards the promotion of neuronal differentiation.

2. Materials and Methods

2.1. Preparation of PLLA-based nanofibers and SEM analysis

PLLA-based nanofibers were produced by electrospinning as follows. A 2% wt/wt polymer solution in a mixture of dichloromethane (DMC; Sigma-Aldrich) and n,n-dimethyl-formamide (DMF; Sigma-Aldrich) was prepared. PLLA pellets were first dissolved in DMC at 30 ºC. After complete dissolution, DMF was added to a final DMC:DMF 70:30 proportion. PLLA solution was electrospun in a Nanon-01A electrospinning machine (MECC CO., LTD, Japan). The solution was poured in a plastic syringe and the feeding processed through a 27-G needle (inner diameter ±0.41 mm) at a 0.5 mL/h feeding rate. The needle-to-collector distance was established to 15 cm and voltage about 15 kV were applied. PLLA-based nanofibers were produced using a collector rotation speed of 150 rpm.

The morphology of the PLLA nanofibers was examined by scanning electron microscopy (SEM) (Hitachi S-4100, Japan) at a 25 kV accelerating voltage, using gold-sputtered samples. The average fibers' diameter was determined from SEM photos by selecting arbitrary areas of the meshes and measuring 200 fibers in 5000× magnified SEM micrographs (Digital Micrograph® software). The diameter of larger fibers was calculated as an average of 30 measurements.

Before cell seeding, PLLA nanofibers were cut into squares of 1 cm × 1 cm and sterilized with 70% ethanol for 5 min. Following one wash with distilled water and two with phosphate buffer saline (PBS), the materials were allowed to dry in the laminar flux chamber.

2.2. Laminin coating

PLLA-based nanofibers and control wells (made of polystyrene) were coated with laminin following the physical adsorption method [22]. For that, control plates and PLLA nanofibers in wells were incubated overnight at 4 ºC in a 10 μg/mL laminin solution that was prepared by diluting a stock solution (Sigma-Aldrich) in sterile PBS. After removing the laminin solution from the well and before use, the samples were washed with sterile PBS and water for 5 min, which allowed the meshes to deposit at the bottom of the wells without floating.

2.3. SH-SY5Y neuroblastoma cells expansion

The neuroblastoma SH-SY5Y cell line (ATCC, Barcelona, Spain; CLR-2266) was maintained at 37 ºC in a humidified atmosphere of 5% CO2, in 10% fetal bovine serum (FBS) minimal essential medium (MEM):F12 (1:1), with 2 mM L-glutamine, 100 U/mL penicillin and 100 mg/mL of a Streptomycin/Penicillin/Amphotericin solution (Gibco). Cells were split at 70–80% confluence.

2.4. Cell adhesion assay

The ability of PLLA nanofibers to promote SH-SY5Y cells adhesion was initially tested [22]. For that, 1×10^5 cells/cm^2 were seeded on previously sterilized nanofibers, coated or not with laminin, and left at 37 ºC in a humidified atmosphere of 5% CO2 for 2 h. After that, cell media were collected to count the number of non-adherent cells using the Trypan blue assay. The percentage of adherent cells was subsequently calculated based on the number of cells initially seeded (taken as 100%).

2.5. Protein identification and quantification by nano-HPLC-MALDI-TOF/TOF

The effects of PLLA-based nanofibers were evaluated using mass spectrometry. SH-SY5Y cells were cultured for 11 days onto PLLA-based nanofibers, collected with boiling 1% SDS, and mass-normalized aliquots of these lysates were subjected to electrophoresis on a 5–20% gradient SDS-PAGE. The resulting gel was incubated with the Brilliant Blue G (Sigma) staining solution for 20 min to visualize and mark bands, and further washed out with the distaining solution overnight until the background was clear. Afterwards, bands of interest were cut out of the gel using a sterile scalpel and kept at −20 ºC for further analysis. Protein bands manually excised from SDS-PAGE gel were destained with 25 mM ammonium bicarbonate/50% acetonitrile and dried under vacuum (SpeedVac®, Thermo Savant, USA). The dried gel pieces were rehydrated with 25 µL of 10 µg/mL trypsin (Promega V5111) in 50 mM ammonium bicarbonate and digested ON at 37 ºC. Tryptic peptides were extracted from the gel with 10% formic acid/50% acetonitrile, dried in a vacuum concentrator and re-suspended in 10 µL of a 50% acetonitrile/0.1% formic acid solution. Separation of tryptic peptides by nano-HPLC was performed on the module separation Ultimate 3000 (Dionex, Amsterdam) using a capillary column (Pepmap100 C18; 3 µm particle size, 0.75 µm internal diameter, 15 cm in length). A gradient of solvent A [water/acetonitrile/trifluoroacetic acid (98:2:0.05, v/v/v)] to solvent B [water/acetonitrile/trifluoroacetic acid (10:90:0.045, v/v/v)] was used. The separation of 2 µg/µL sample was performed using a linear gradient (5–50% B for 30 min, 50–70% B for 10 min and 70–5% A for 5 min) with a flow rate of 0.3 µL/min. The eluted peptides were mixed with a continuous flow of α-CHCA matrix solution (270 nL/min, 2 mg/mL in 70% ACN/0.1% TFA and internal standard Glu-Fib at 15 ftmol) and applied directly on a MALDI plate in 7 seconds fractions using an automatic fraction collector Probot (Dionex, Amsterdam).

Mass spectra were obtained on a matrix-assisted laser desorption/ionization-time-of-flight MALDI-TOF/TOF mass spectrometer (4800 Proteomics Analyzer, Applied Biosystems, Foster City, CA, USA) in the positive ion reflector mode and obtained in the mass range from 700–4500 Da with 900 laser shots. Glu-Fib was used for internal calibration. A data-dependent acquisition method was created to select the 16 most intense peaks in each sample spot (considering 2 spots per fraction) for subsequent tandem mass spectrometry (MS/MS) data acquisition, excluding those from the matrix,

due to trypsin autolysis or acrylamide peaks. A fragmentation voltage of 2 kV was used throughout the automated runs. The spectra were processed and analyzed by the T2S (v1.0, Matrix Science Ltd, U.K.) and submitted in Mascot software (v.2.1.0.4, Matrix Science Ltd, U.K.) for protein/peptide identification based on MS/MS data using the following criteria: trypsin as enzyme; a maximum of two missed cleavages; mass tolerances of 20 ppm for peptide precursors, mass tolerance of 0.3 Da was set for fragment ions. Protein identifications based on MS/MS data were considered as reliable when the Mascot ion score confidence level for each individual peptide was > 32. The local FDR (False Discovery Rate) was calculated by searching the spectra against SwissProt (Homo sapiens, release date 01052013) decoy (random) database. Quantification was performed using exponentially modified protein abundance index (emPAI) values, which is based on equation 1 [24]: $[emPAI = 10^{\frac{Nobserved}{Nobservable}} - 1]$, where "N observed" is the number of experimentally observed peptides and "N observable" is the calculated number of observable peptides, for each protein. Normalization to the total number of peptides in the sample was also performed.

2.6. Bioinformatics analyses of cellular pathways

The lists of proteins altered by SH-SY5Y-nanofibers interaction, as determined by MS/MS data, were used for gene ontology and pathway enrichment analyses in Panther [25] and Reactome v57 [26,27], respectively. Reactome analysis was performed with the option to include IntAct interactors to increase the analysis background; the Reactome analysis of down-regulated proteins is presented graphically in Figure 3. From these, the statistically significant ($p < 0.05$) or near significant ($p \approx 0.05$) enriched signaling pathways were selected and listed in Table 3. Of note, no statistically significantly enriched signaling pathways were retrieved with the lower number of up-regulated proteins ($p > 0.05$).

2.7. Cellular viability assay

To evaluate the ability of PLLA nanofibers to support cell growth and proliferation, the resazurin viability assay was performed. For that, the properly sterilized and coated squared-shaped PLLA nanofibers were placed on 24-well plates. A total of 5×10^4 SH-SY5Y cells/2 cm^2 were subsequently seeded on the nanofibers or directly on the culture plate bottom ("Control"). At the indicated time points (2nd, 5th, 8th and 11th day) cells were incubated for 4 h with fresh medium containing 10% of a 0.1 mg/mL resazurin (Sigma-Aldrich) in PBS (Pierce, Thermo Scientific). Resazurin reduction to resorufin was thereafter measured by spectrophotometry (microplate reader Infinite 200 PRO Tecan, Grupo Taper, Portugal) at 570 nm (resazurin maximum absorbance) and 600 nm (resorufin maximum absorbance). For each day, a final optical density value (O.D.f) was calculated as follows:

$$ODf = Sample\ \left(\frac{OD_{570nm}}{OD_{600nm}}\right) - Negative\ Control\ \left(\frac{OD_{570nm}}{OD_{600nm}}\right)$$

where the negative control is the O.D. of resazurin in the absence of cells.

2.8. Immunoblot analyses of protein levels

At the end of the viability assay (11th day) cells were harvested in 1% boiling SDS and subjected to immunoblot analyses as previously described [28]. Briefly, mass-normalized aliquots (using the BCA protein assay kit, Pierce's, Thermo Scientific) were electrophoresed on a 5–20% gradient

SDS-PAGE and transferred onto nitrocellulose membranes. Ponceau S reversible staining was first performed to detect total protein content, membranes further scanned in a GS-800™ Calibrated Densitometer (Bio-Rad) and band intensities quantified (Quantity One densitometry software, Bio-Rad) for subsequent relative total protein loading corrections [29]. For immunoblotting, the following primary antibodies were used diluted in 3% bovine serum albumin (BSA)/in Tris-buffer saline with Tween (TBS-T): pan-antibody to Actin (1:10; Acris); anti-β-Tubulin antibody (1:2000; 2-28-33, Invitrogen); anti-PARP (214/215) cleavage site (1:1000; Millipore), and anti-PARP antibody (1:1000; Thermo Scientific, Fischer Scientific). Horseradish-peroxidase secondary antibodies (1:5000; GE Healthcare) were used for enhanced chemiluminescence (ECL) detection, using homemade or Luminata^{TM} Crescendo (Millipore) ECL solutions. Quantity One densitometry software (Bio-Rad) was then used to quantify the band intensities using Ponceau S lane levels as a loading control.

2.9. Microscopy analysis of undifferentiated and differentiated cells

The effects of the PLLA materials on undifferentiated SH-SY5Y cells morphology and spreading were assessed at the end of the viability assay (11th day). Briefly, cells grown on coverslips or on PLLA platforms were fixed with a 4% paraformaldehyde (PFA) in PBS solution and permeabilized with 0.1% Triton/PBS. Fixed cells were incubated for 20 min in the dark with Alexa Fluor 568 Phalloidin (Invitrogen) (1:50 in 1% BSA/PBS) to stain filamentous actin (F-actin), and mounted with the DAPI-plus VECTASHIELD® (Vector Laboratories) on 0.1 mm microscope glass slides for analysis in an Olympus IX-81 inverted epifluorescence microscope (LCPlanFl 20x/0.40 objective).

The same procedure was applied to analyze the effects of PLLA nanofibers on SH-SY5Y cells cultured for two days with 10 μM Retinoic Acid (RA) in 10% FBS medium, to evaluate the effects of the nanofibers on the onset of neuron-like SH-SY5Y differentiation.

2.10. Data analysis

Data is expressed as mean ± SE (standard error) of at least three independent experiments. Statistical significance analysis was conducted by one way analysis of variance (ANOVA) followed by the Tukey's test (if samples' SE were statistically different) or Welch's test (if samples' SE were non-statistically different).

3. Results and Discussion

3.1. PLLA nanofibers morphology and cellular adhesion

PLLA scaffolds are piezoelectric biodegradable materials that when electrospun as nanofibers can provide topographic cues known to promote differentiation [2,3]. In this work we explored the cellular responses elicited by PLLA-based nanofibers ("NanoF") that might underlie their ability to promote neuronal differentiation.

Electrospun NanoF were first characterized by scanning electron microscopy (SEM), and their ability to support SH-SY5Y cells adhesion was further confirmed. NanoF SEM micrographs are presented in Figure 1a. The electrospun fibers-based platforms presented a thickness around 150 μm with nanometer-sized fibers, with an average diameter size of 468 ± 165 nm. Although a lower

diameter size (e.g. to 200–300 nm) has shown to improve neuronal differentiation [18] we verified that lowering the PLLA concentration in the solution led to instability of the charged jet during the electrospinning process and subsequently to a mesh with higher heterogeneity of fibers' sizes. The NanoF platforms also presented some larger fibers, 0.97 ± 0.36 µm of average diameter size, which may result from fibers merging. To assess the influence of NanoF on SH-SY5Y cell adhesion, the number of cells that did not adhere after 2h of culture onto empty plates or onto laminin-coated or uncoated NanoF were quantified. Laminin is an extracellular matrix (ECM) protein known to promote neuronal adhesion and differentiation [22]. Figure 1b presents the percentage of adherent cells and reveals that NanoF, with or without surface modification such as laminin-coating, are able to support SH-SY5Y cell adhesion in the same extend as plastic dishes (Control conditions).

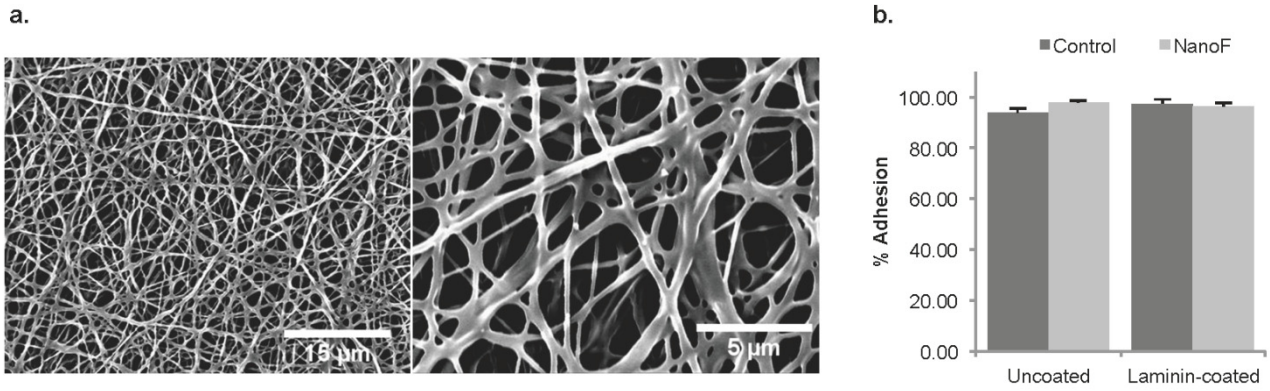

Figure 1. Surface morphology of PLLA-based nanofibers and adhesion of SH-SY5Y cells. a. SEM micrographs showing the morphology of PLLA-based surfaces. **b.** Cell adhesion assay of SH-SY5Y to PLLA-based nanofibers (NanoF) compared to control condition (plastic bottom of the culture dish). A total of 1×10^5 cells/cm^2 were seeded on uncoated and laminin-coated PLLA nanofibers in a 24-well cluster plate. After 2 h of cell adhesion, the number of non-adherent cells in the media was scored and the percentage of adherent cells was indirectly inferred. $n = 6$.

3.2. Effects of PLLA nanofibers on the SH-SY5Y cells proteome and pathways

After validating the adhesion of SH-SY5Y cells to NanoF, mass spectrometry was used to assess the effects of NanoF on SH-SY5Y cells' proteome and corresponding cellular pathways. The hypothesis that NanoF induces alterations in SH-SY5Y cells proteome was already suggested by altered protein profiles in the lysates of cells grown on PLLA platforms, evidenced in total protein staining (Figure 2a). In particular, two bands (at ~60 and 70 kDa) seemed more intense in the lysates of cells grown on the NanoF, whereas other NanoF bands (at ~80 and 100 kDa) were slightly fainter. These exact alterations also occurred in SH-SY5Y lysates of cells grown on other PLLA-based platforms, namely solvent-casted films and electrospun scaffolds with aligned nanofibers (data not shown).

Mass spectrometry analysis of the four extracted bands (60, 70, 80 and 100 kDa; arrowheads in Figure 2a) identified 185 different proteins. From these, only 83 proteins had at least 2 hints in each of the conditions (Control or NanoF). The *emPAI* was then used as an indicator of protein abundance within the sample, enabling protein classification as "up- or down-regulated". Of these 83, 38 were found to be equally expressed in Control and NanoF samples, 12 were up-regulated in NanoF

conditions (increased in NanoF, when compared to Control, or exclusively found in NanoF), and 33 were down-regulated in NanoF (decreased in NanoF, when compared to Control, or exclusively found in Control samples) (Table 1, Supplementary Table S1).

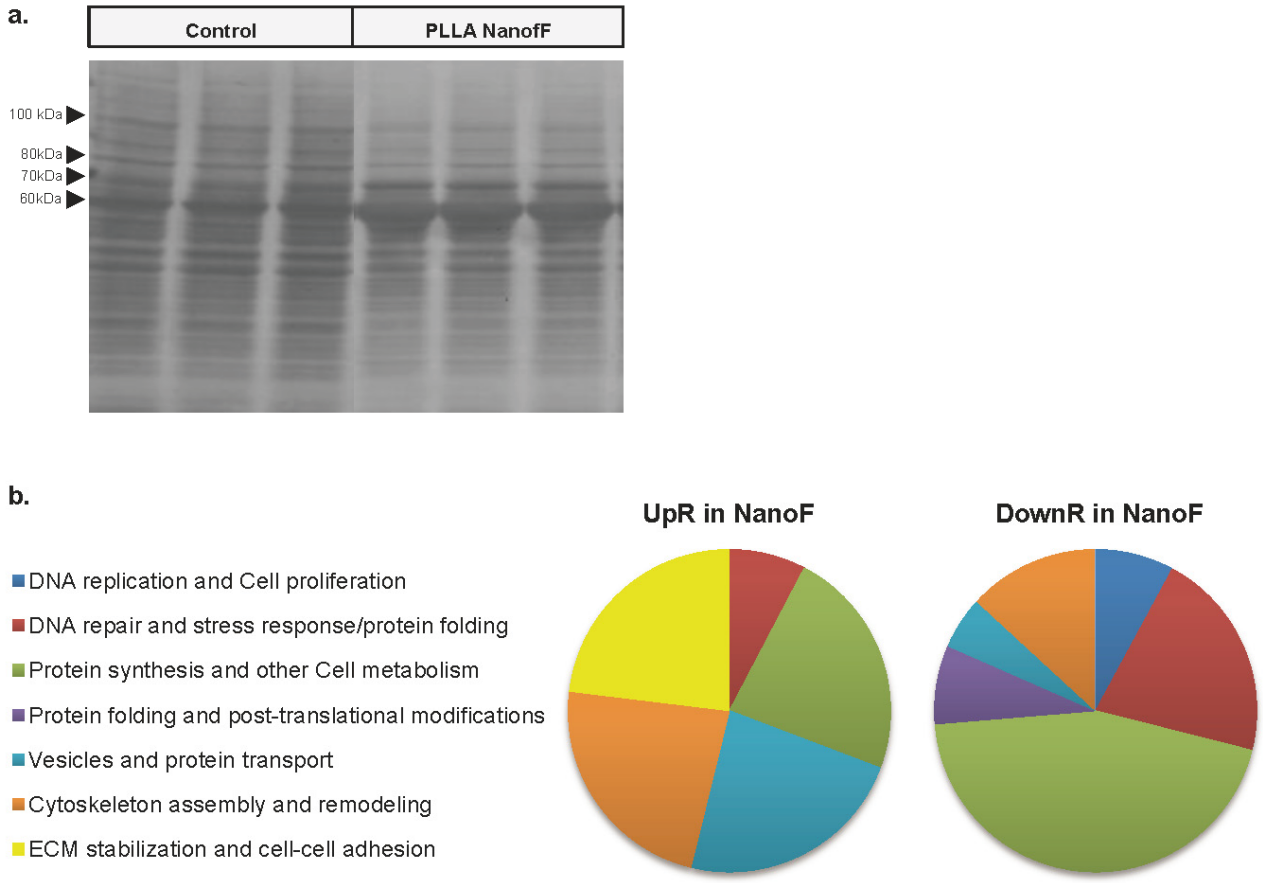

Figure 2. Influence of the PLLA nanofibers on the SH-SY5Y cell proteome and cellular functions up- and down-regulated. a. Ponceau staining of total proteins present on the nitrocellulose membrane. Triplicates of cell lysates cultured on PLLA NanoF or directly on the plate ('Control') were run side-by-side in a SDS-PAGE. Protein staining with Ponceau S revealed sets of protein bands increased or decreased in cells grown on PLLA nanofibrous platforms. The bands indicated by their average molecular weight, kDa, were excised from the gel and their protein content analyzed by mass spectrometry. **b.** 45 proteins were identified by mass spectrometry analysis of cells cultured on NanoF for 11 days, whose levels were altered (either increased or decreased). Their cellular function was determined and categorized into the cellular mechanisms presented in the color-coded pie charts.

The functional processes and pathways in which the identified up- and down-regulated proteins are involved were further explored (Figure 2b). The functional pie charts revealed that cells grown on NanoF shift their protein expression towards a more plastic differentiation-supportive state, contrary to the more proliferative-state observed in Control cells. Up-regulated proteins in cells grown on NanoF are mainly involved in cellular pathways that play a role in cell metabolism, protein

trafficking, cytoskeleton assembly and remodeling, and in ECM stabilization. Proteins that are down-regulated by NanoF are mostly involved in pathways underlying cell division and DNA replication, DNA expression and protein synthesis, cell metabolism, DNA repair and stress response.

Table 1. Summary of proteins identified through mass spectrometry analysis in SH-SY5Y cells cultured on PLLA nanofibers (NanoF) and on control (glass coverslips).

Band	Identified proteins	Equal emPAIs	Different emPAIs			
			Upregulated in NanoF		Downregulated in NanoF	
			Unique in NanoF	UpR in NanoF	Unique in Control	DownR in NanoF
100 kDa	29	11	4	2	4	7
80 kDa	38	22	3	3	3	6
70 kDa	40	17	4	4	2	8
60 kDa	27	13	0	2	5	6
Total	83	38	6	6	13	20
			12		33	

Identified proteins: the number of proteins identified in each gel band of indicated molecular weight (kDa). These proteins were classified as: "Unique", proteins found in all samples of only one of the conditions (Control or NanoF); "UpR", upregulated proteins, proteins whose emPAI value is higher in duplicates or triplicates of the NanoF condition in comparison with the duplicates or triplicates of the Control condition. "DownR", downregulated proteins, NanoF proteins with an emPAI value lower than the Control condition. Protein expression was considered altered if the Mascot score > 32 and the protein was identified in at least two samples of the same condition (Control or NanoF).

Table 2 describes the ID and the function of relevant proteins found altered by NanoF by the mass spectrometry analysis, also relating them to Figure 2b. Up-regulated proteins in SH-SY5Y cells grown on NanoF include proteins involved in cell metabolism, in agreement with most recent findings that PLLA nanofibers increase the cellular energetic metabolism [20]. Further, three interesting proteins involved in neural development, cell-cell adhesion (and cell proliferation inhibition) and actin remodeling were also up-regulated by NanoF. Alpha-2-HS-glycoprotein (alias Fetuin) is secreted by stem cell-derived skin lineage precursors and participates in endocytosis and in extracellular matrix formation [30], being involved in bone and brain development [31]. Inter-alpha-trypsin inhibitor heavy chain H2 is a protein that bridges hyaluronan and other matrix proteins, and was observed to block glioma cells invasion, inhibit their proliferation and to promote cell-cell adhesion, partially via the phosphatidylinositol 3-kinase/Akt signaling cascade [32]. Gelsolin, found three-fold increased, has a major role in actin remodeling as it induces the nucleation of actin monomers to form new actin filaments, and the severing of already formed filaments [33,34].

Regarding the down-regulated proteins, a major part is involved in chromatin organization, DNA replication and repair, and gene expression. These include KHDR1, a regulator of the cell cycle progression [35]; MCM5, a putative helicase involved in DNA replication facilitation [36]; and Prelamin-A/C, which participates in nuclear assembly and structural maintenance, and in chromatin organization [37,38]. Two proteins involved in pre-mRNA metabolism are also down-regulated: Heterogeneous nuclear ribonucleoprotein U (HNRPU) and a putative RNA helicase (DDX5), potentially involved in the regulation of pre-mRNA splicing [39,40].

Table 2. Identity of proteins identified by MS/MS with different expression on Control and NanoF samples.

Accession number	Protein name	Molecular weight[1]	Fold increase	Cellular function	Ref.
P06396 GELS_HUMAN	Gelsolin	87 kDa	3.27*	Cytoskeleton assembly and remodeling (nucleation of actin monomers into filaments and severing of already formed filaments)	[33,34]
P02765 FETUA_HUMAN	Alpha-2-HS-glycoprotein	39 kDa	1.52	ECM stabilization (extracellular matrix maturation, brain development, endocytosis)	[30,31]
P19823 ITIH2_HUMAN	Inter-alpha-trypsin inhibitor heavy chain H2	106 kDa	1.75	ECM stabilization (intermediate protein between hyaluronan and other matrix protein; inhibitor of neural cells proliferation and inducer of cell-cell adhesion)	[32]
P17844 DDX5_HUMAN	Probable ATP-dependent RNA helicase DDX5	69 kDa	0.33	Protein synthesis (involved in the alternative regulation of pre-mRNA splicing)	[39]
Q16643 DREB_HUMAN	Drebrin	71 kDa	0.31*	Cytoskeleton assembly and remodeling (required for actin polymerization, cell migration and neuronal plasticity	[47]
Q14195 DPYL3_HUMAN	Dihydropyrimidinase-related protein 3	62 kDa	0.46	Cytoskeleton assembly and remodeling (regulation of neuronal growth cone collapse via semaphorins signaling)	[63]
P11021 GRP78_HUMAN	78 kDa glucose-regulated protein	72 kDa	0.46	Protein folding (ER chaperon; assembly of multimeric protein complexes)	[41,42]
P08238 HS90B_HUMAN	Heat shock protein HSP 90-beta	83 kDa	0.41	Cell proliferation (also protein folding) (regulation of proteins involved in cell cycle and signal transduction; chaperon)	[41]
P02545 LMNA_HUMAN	Prelamin-A/C	74 kDa	0.32*	DNA replication (nuclear assembly and chromatin organization)	[37,38]
P09874 PARP1_HUMAN	Poly [ADP-ribose] polymerase 1	113 kDa	0,36	DNA repair (reparation of DNA strand breaks and transcription regulator)	[43,44]
Q00839 HNRPU_HUMAN	Heterogeneous nuclear ribonucleoprotein U	91 kDa	0.61	Protein synthesis (pre-mRNA processing, mRNA metabolism and transport)	[40]
Q07666 KHDR1_HUMAN	KH domain-containing, RNA-binding, signal transduction-associated protein 1	48 kDa	0.50	Cell proliferation (role in G2-M progression in cell cycle)	[35]
P33992 MCM5_HUMAN	DNA replication licensing factor MCM5	82 kDa	0.57	DNA replication (component of the MCM complex, a putative	[36]

				replicative helicase, function in DNA replication initiation and elongation)	
P35241 RADI_HUMAN	Radixin	69 kDa	0.64	Cytoskeleton assembly and remodeling (member of the ERM actin regulator proteins. Anchorage of the plasma membrane and the actin cytoskeleton)	[48]
Q13263 TIF1B_HUMAN	Transcription intermediary factor 1-beta	89 kDa	0.23	Protein synthesis (regulator of DNA transcription)	[45,46]

The main proteins whose levels were found altered in cells grown for 11 days on PLLA nanofibers and identified in at least 2 samples of each condition (Control or NanoF) are listed. The Fold Increase (FI) was calculated based on the emPAI, indicator of the protein abundance in the sample; positive FI: up-regulated protein in cells grown on NanoF; negative FI: down-regulated protein in cells grown on NanoF. Asterisk (*) indicates statistical significance ($p < 0,05$) of the fold increase; the majority of the proteins is only tendentiously up- or down-regulated. The function of the identified proteins is based on information contained in the indicated references (Ref.).
[1]Protein molecular weight without considering post-translational modifications.

NanoF also down-regulated stress-related chaperones such as HSP90 and GRP78 [41]. The later is also involved in the regulation of the cell cycle and apoptosis [42], as the DNA stress-induced Poly (ADP-ribose) polymerase 1 (PARP1) protein, involved in DNA strand reparation and regulation of DNA transcription [43,44]. Like PARP1 (3-fold decreased), the Transcription intermediary factor 1-beta (TIF1B) [45,46] is also downregulated (4-fold decreased).

Other proteins involved in cytoskeleton polymerization and stabilization, and neuronal growth cone collapse, were also decreased (Table 2). Drebrin (DREB), for instance, is involved in actin polymerization and neuronal plasticity [47]; Radixin (RADI) is a member of the Ezrin-Radixin-Moesin (ERM) actin regulators, well-known to regulate actin polymerization. ERM are a class of highly homologous proteins that structurally and functionally link the plasma membrane to the cortical F-actin cytoskeleton [48]. The also decreased Dihydropyrimidinase-related protein 3 (DPYL3) is involved in the semaphorins signaling for neuronal growth cone collapse.

Various signaling pathways were also found hindered by NanoF exposure when the interaction network of the downregulated proteins was expanded using the Reactome software. Figure 3 shows near the same cellular processes as the ones obtained with the Panther software (Figure 2b), plus various signaling pathways. From these, enriched signaling pathways ($p <$ or ≈ 0.05) were selected and listed in Table 3. Concordantly with the functional analyses of main altered proteins, the majority of the pathways is involved in cell proliferation, being related to growth factors and their receptors (Table 2). These comprise the Vascular endothelial growth factor (VEGF) [49], the Fibroblast growth factor receptors 1 and 2 (FGFR1 and FGFR2) [50], the Epidermal growth factor receptor (EGFR) [51], and the EGFR-interactor and regulator Protein-tyrosine kinase 6 (PTK6, alias Brk) [52]. Two other pathways, related to cellular stress (NLR signaling pathway) and growth cone collapse, were also inhibited by NanoF. Central to the first pathway are the Nucleotide-binding domain, leucine rich repeat containing receptor (NLR) and many of its family members. These are involved in inflammasome complexes in human cells in response to stress and may induce caspase activation [54]. The second one, the Sem3A semaphorin signaling, is a known pathway that mediates the collapse of the growth cones at the tips of growing neurites in differentiating and regenerating neurons [54].

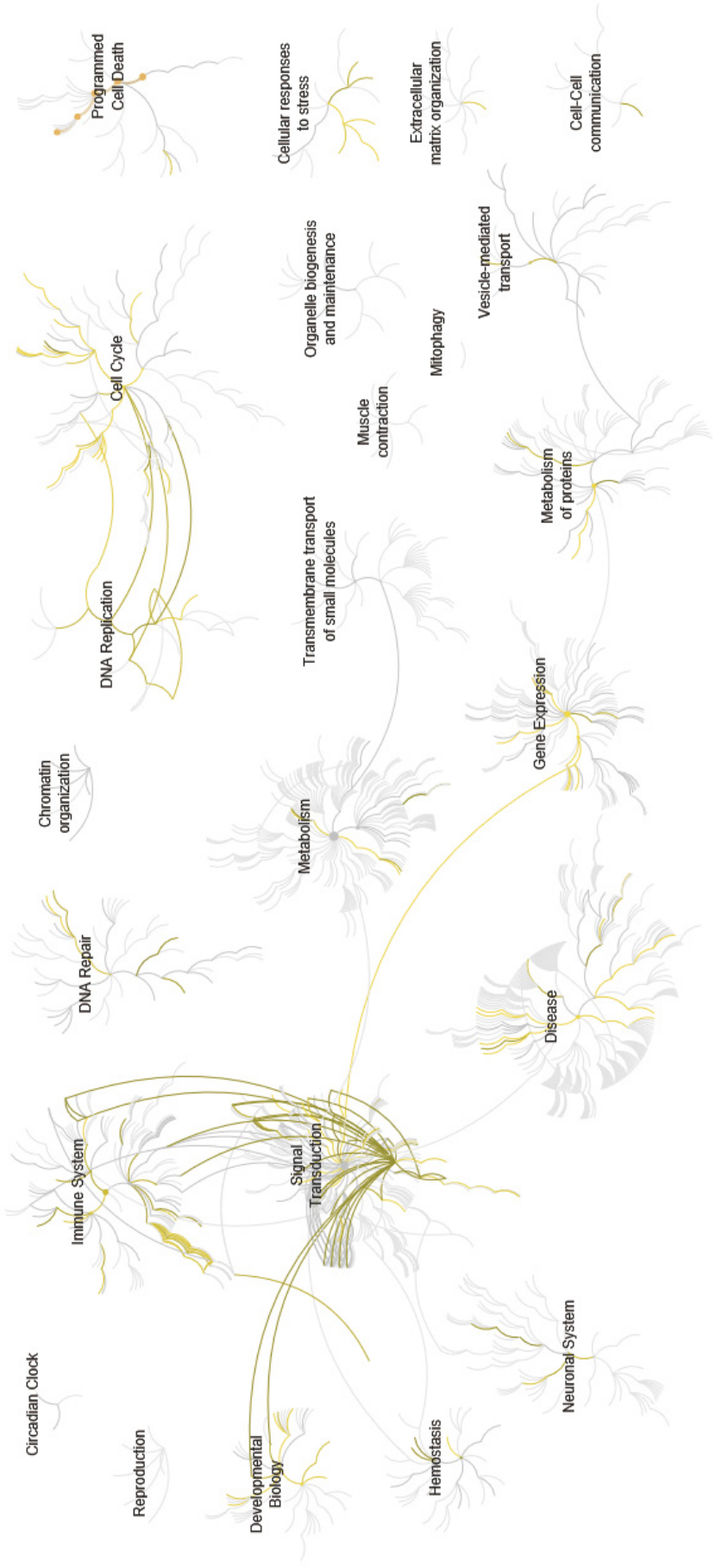

Figure 3. Extended network of SH-SY5Y proteins down-regulated by PLLA-based nanofibers. Proteins and their interactors were distributed in biological pathways and represented graphically using the Reactome analysis tool.

Table 3. Signaling pathways identified as significantly down-regulated by PLLA nanofibers.

Pathway name	Entities pValue	Entities FDR	Submitted entities found	Submitted entities hit interactor	Interacts with
Signaling by VEGF	0.0018	0.0106	HS90A_HUMAN	HS90B_HUMAN;KHDR1_HUMAN;U5S1_HUMAN;GRP78_HUMAN;HS90A_HUMAN;HSP71_HUMAN;HSP7C_HUMAN	P04049;P07900;P35916;P31749;P19174;P53041;P06241;P15056;P04792
Signaling by PTK6	0.0074	0.0252	KHDR1_HUMAN	HS90B_HUMAN;KHDR1_HUMAN;GRP78_HUMAN;HS90A_HUMAN;HSP7C_HUMAN	Q5S007;P31749;Q07666
CRMPs in Sema3A signaling	0.0088	0.0265	DPYL2_HUMAN; DPYL3_HUMAN	-	-
Cytokine Signaling in Immune system	0.0316	0.0537	NUP93_HUMAN	MCM7_HUMAN;HS90B_HUMAN;KHDR1_HUMAN;KINH_HUMAN;GRP78_HUMAN;HS90A_HUMAN;LMNA_HUMAN	P04049;Q99558;P15498;P41279;P19838;P07948;P53041;P15056;P63104
Signaling by Ligand-Responsive EGFR Variants in Cancer	0.0353	0.0537	HS90A_HUMAN	KHDR1_HUMAN	P19174
Constitutive Signaling by Ligand-Responsive EGFR Cancer Variants	0.0353	0.0537	HS90A_HUMAN	KHDR1_HUMAN	P19174
Nucleotide-binding domain, leucine rich repeat containing receptor (NLR) signaling pathways	0.0354	0.0537	HS90B_HUMAN	MCM7_HUMAN;HS90B_HUMAN;HS90A_HUMAN	Q9Y6K9;P08238;Q9Y239
Signal Transduction	0.0547	0.0547	HNRPM_HUMAN; PARP1_HUMAN; KHDR1_HUMAN; KINH_HUMAN; HS90A_HUMAN	MCM7_HUMAN;HS90B_HUMAN;PARP1_HUMAN;HS90A_HUMAN;SF3A1_HUMAN;LMNA_HUMAN;GANAB_HUMAN;TIF1B_HUMAN;KHDR1_HUMAN;DDX5_HUMAN;U5S1_HUMAN;HNRPU_HUMAN;KINH_HUMAN;GRP78_HUMAN;HSP71_HUMAN;HSP7C_HUMAN;NUP93_HUMAN	P04049;Q13546;Q13547;P05412;P49674;P31749;O15111;P31946;Q07666;P06241;P09874;P09651;P08047;Q01974;P15498;Q9UNE7;P46527;Q12933;P36896;P15056;Q09472;P07900;P35916;Q5S007;P19174;P00533;Q15831;P01106;Q13573;P63104;P04792;P42679;P53041;P32121;P31152
Signaling by FGFR2	0.0561	0.0561	HNRPM_HUMAN	HS90B_HUMAN;KHDR1_HUMAN;GRP78_HUMAN;HS90A_HUMAN	P04049;P31749;O15111;P19174;P53041;P15056;P09651

Signaling by FGFR	0.0579	0.0579	HNRPM_HUMAN	HS90B_HUMAN;KHDR1_HUMAN ;GRP78_HUMAN;HS90A_HUMAN	P04049;P31749;O15111; P19174;P53041;P15056; P09651

The SH-SY5Y down-regulated proteins ("submitted entities") identified in the MS/MS data were analysed using the bioinformatics tool Reactome upon extending their network of interactors. Significantly enriched ($p < 0.05$) signaling pathways are listed here. "Entities found": the curated and interacting molecules that are common between the submitted data set and the pathway named. "Submitted entities hit interactor" (interactors found): IntAct-interacting molecules that are common between the submitted data set and the pathway named. "Interacts with": other interacting molecules that are not listed in the submitted data set.

3.3. The effect of PLLA nanofibers on cellular proliferation and apoptosis

The mass spectrometry data suggested that NanoF induced a decrease in SH-SY5Y cells proliferation. The influence of the PLLA platforms on the number of SH-SY5Y cells with time in culture was assessed via the non-destructive metabolic Resazurin assay (Figure 4a). Uncoated and laminin-coated PLLA platforms were evaluated. An effect of inhibition of neuroblastoma cell number was confirmed to exist for the NanoF condition. A decrease in cells proliferation is evident from the proliferation curves of SH-SY5Y cells grown on NanoF (Figure 4a). This is concordant with all functional analyses of the MS/MS proteomic results, including the findings that cell proliferation signaling pathways such as the VEGF, FGFR, and EGFR, were inhibited (Table 3). Laminin-coating similarly decreased cell proliferation (Figure 4a), as expected since laminin is an ECM protein that influences cellular processes including survival, proliferation and differentiation [22]. NanoF may similarly influence these processes as it mimics the ECM nanoarchitecture [55].

According to the MS/MS data, one of the proteins whose levels were highly decreased by NanoF is PARP1 (Table 2). PARP (117 KDa) is a crucial protein regulating the cell cycle and DNA repair, which is cleaved by caspase 3 and 7 during apoptosis, yielding two fragments of 85 and 25 kDa [43,44]. The MS/MS analysis of the 80 kDa band suggests that PARP and/or its cleavage ~85 kDa fragment are decreased in NanoF-cultured cells. Full-length PARP is more indicative of cell division and DNA repair, while the ratio between PARP cleaved and full-length forms is an indirect measure of apoptosis. The levels of full length PARP1 (117 KDa) and of its apoptosis-induced cleaved fragment were measured (Figure 4b). Cells cultured on NanoF presented a consistently decreased ratio of PARP cleavage into the 85 kDa fragment (Figure 4b, cleaved/full length PARP ratio), either in uncoated or in laminin-coated NanoF. Laminin-coated NanoF always presented the lowest values of full-length and cleaved PARP, in what appears a synergistic action of the nanofibers' topography and the ECM coating. These results first confirm the PARP1 data from the MS/MS proteomic analysis (Table 2) and suggest lower cellular apoptosis for cells grown on NanoF. Furthermore, it confirms that the previously observed decreases in cell density (Figure 4a) are not due to increased apoptosis but rather to lower cell proliferation, as already suggested by the bioinformatics functional analyses to the MS/MS data (Figures 2b and 3, Tables 2 and 3).

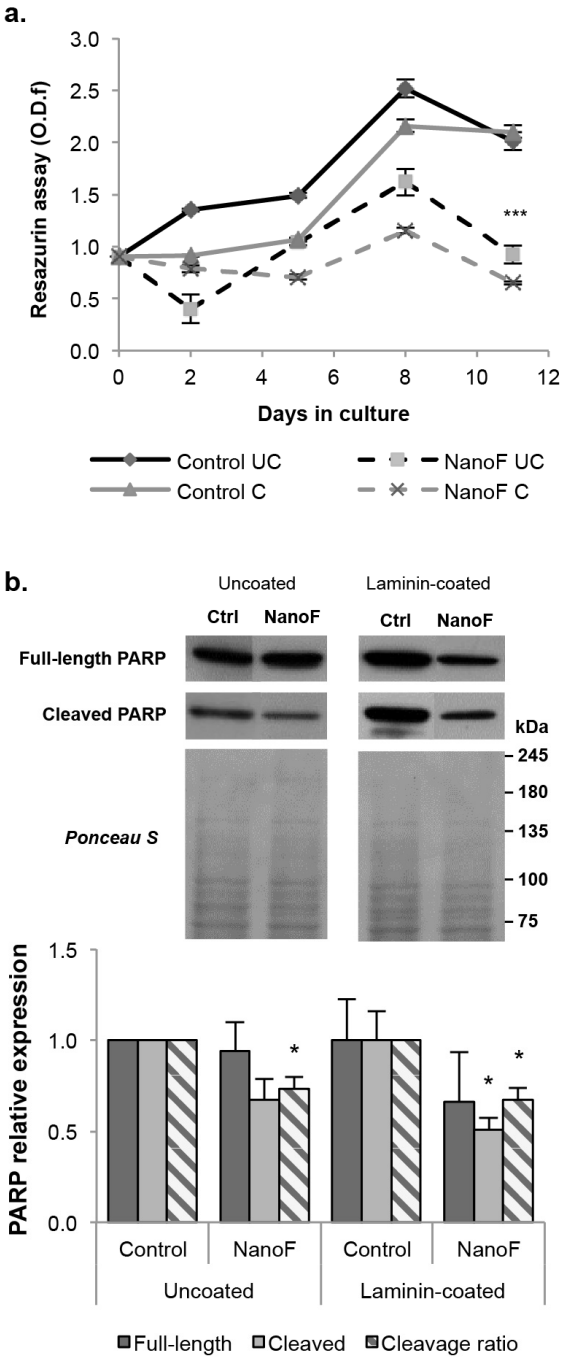

Figure 4. Effect of PLLA-based nanofibers on cell viability and apoptosis. a. Cell viability resazurin assay of SH-SY5Y cells cultured for 11 days on uncoated and laminin-coated PLLA-based nanofibers (NanoF) and Control (cells cultured directly on the plastic bottom of the culture plate). Results are depicted as mean optical density (O.D.f) mean ± SE. $n = 6$. ***($p < 0.001$): statistically significant differences between NanoF and control, both in coated (C) and uncoated (UC) conditions at day 11. **b.** Immunoblot analysis of the expression and cleavage of poly (ADP-ribose) polymerase (PARP) at the end of the viability assay (11th day) in the SH-SY5Y cellular lysates. Cleavage ratio, which is an indicator of apoptosis, is given by the division of the cleaved PARP (87 kDa) levels by the full-length PARP (117 kDa) levels. Data was normalized using Ponceau staining as loading control. Mean ± SE, $n = 3–6$. * ($p < 0.05$).

3.4. Effects of PLLA nanofibers on cytoskeleton remodeling and differentiation

Growth characteristics of neurites (as number, morphology, orientation and rate) are determined by environmental cues and cellular mechanisms that involve altered actin and tubulin cytoskeletons dynamics [56]. Actin mediates the establishment of cellular morphology and the interaction with the ECM [57]. Tubulin, less subject to turnover, provides a scaffold for maintaining the extending neurite [57]. Besides inhibition of cell proliferation, NanoF upregulated proteins are also involved in cytoskeleton remodeling, protein trafficking, and cell-cell adhesion. The proteome seems to shift to enable cells to undergo significant morphological alterations that may prepare them for the onset of cellular differentiation [58].

To first evaluate the effects of NanoF on the cytoskeleton and on cells differentiation, the levels of cytoskeleton-related proteins, i.e. actin and tubulin, were assessed (Figure 5a). Actin and tubulin levels were found to decrease in cells grown on NanoF, and accentuated when the platforms were laminin-coated. Subsequently, the morphology of SH-SY5Y cells cultured on NanoF was monitored in non-differentiating conditions (Figure 5b, left panel). The previously observed variations in cell number (Figure 4a) are roughly visually confirmed in the fluorescence images, as NanoF presents a decreased cell number (Figure 5b). In these non-differentiating conditions (left panel), NanoF induced alterations in cell distribution, shape and cytoskeleton rearrangements. NanoF samples increase cell-cell adhesion and alter the cuboid morphology of cells (observed in control conditions) to a round-shaped one. Additionally, NanoF appear to induce the depolymerisation of the filamentous actin (F-actin) in stress fibers, which are the linear arrays of actin bundles that cross the cells (visible in Control cells) (Figure 5b, left panel). Hence, in the absence of differentiating inductors, cells grown on the PLLA nanofibers present an accentuated decrease on actin levels and acquire a rounder morphology with few or no visible stress fibers due to F-actin disruption (Figure 5a, b left panel). Poor spreading in nanofibrous scaffold has been observed in other cell types such as the endothelial cells (HUVECs) [59], and may relate to the NanoF high hydrophobicity (data to be submitted elsewhere). Indeed, hydrophobicity inhibits the formation of mature focal adhesions (FA) and delays cytoskeleton development [60]. Further, NanoF induced the up-regulation of the Inter-alpha-trypsin inhibitor heavy chain H2, which increases cell-cell adhesion [32]. The NanoF-induced disruption of the actin cytoskeleton might be mediated by the down-regulation of actin polymerizing proteins such as Radixin and Drebrin, and the up-regulation of the F-actin remodeling protein, Gelsolin. This calcium-regulated protein severs pre-existing F-actin filaments and caps their growing barbed ends [34]. Gelsolin might be activated by calcium influxes arising from the cells adhesion and adaptation to the nanofibers' surface and subsequent activation of stretch-activated cation channels; these transduce mechanical signals from FAs to the cytoskeleton, that ultimately lead to actin reorganization [61].

Actin remodeling is a known necessary step for cells to acquire a specialized morphology upon differentiation. Moreover, we have previously observed that an early period of drop on tubulin and actin levels occur at the onset of SH-SY5Y neuronal differentiation [21]. We thus hypothesize that the NanoF-induced actin remodeling render cells in a transmorphogenic state [62] that make them more prone to respond to differentiating drugs such as Retinoic acid (RA) (Figure 5c). Concordantly, SH-SY5Y cells grown on NanoF in the presence of RA present a more neuron-like morphology, as these extend a higher number of longer projections than control cells already at 2 days in RA (Figure 5b, right panel). Hence, cells grown on NanoF present an altered morphology and cytoskeleton and are more prone to undergo neuronal differentiation, most possibly due to the intrinsic changes in their

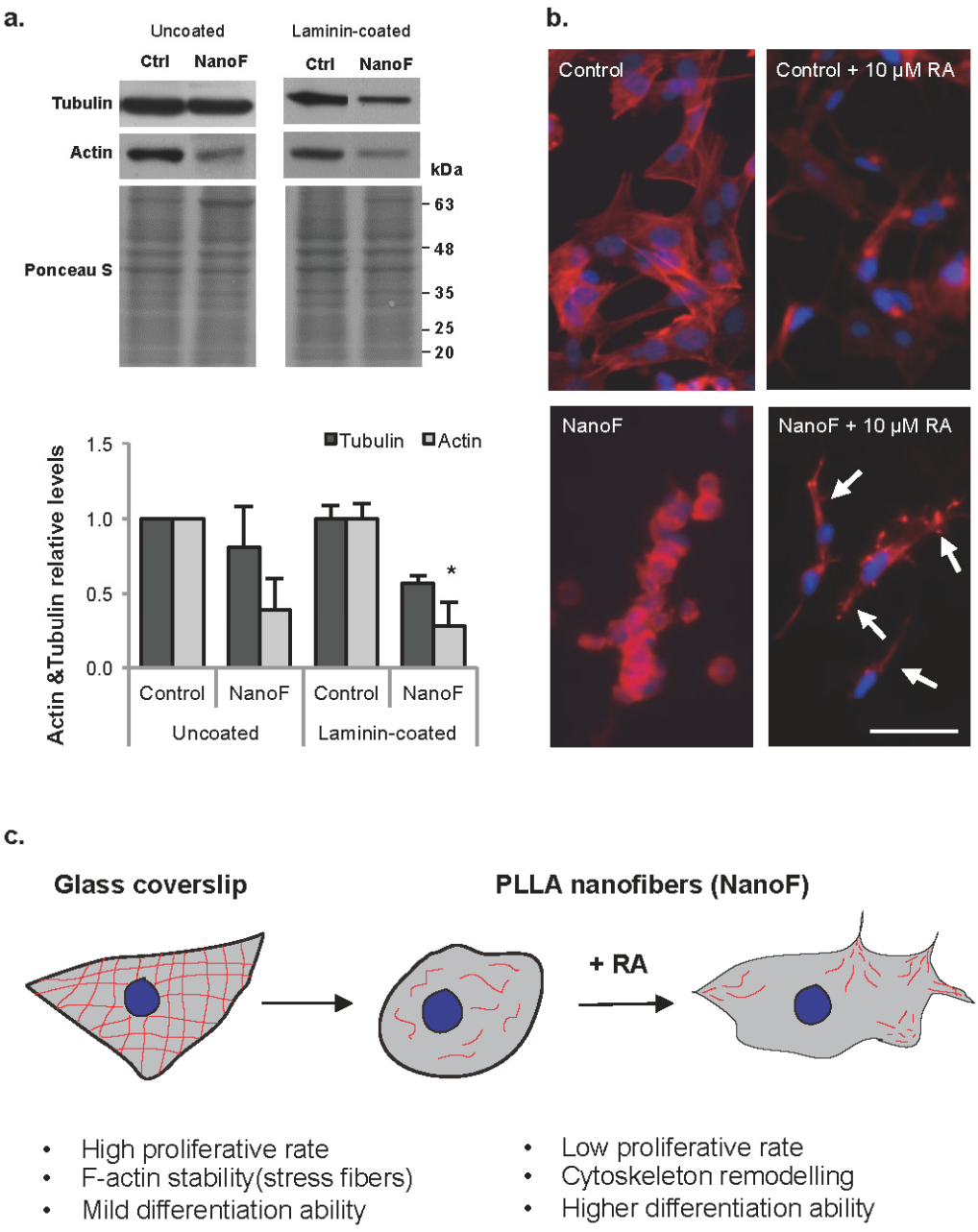

Figure 5. Effect of PLLA-based nanofibers on SH-SY5Y cells' cytoskeleton and differentiation. a. Immunoblot and corresponding graphic analysis of the levels of the cytoskeleton-related proteins Actin (42 KDa) and β-Tubulin (50 KDa), in SH-SY5Y cells cultured for 11 days on laminin-coated or uncoated PLLA-based nanofibers ('NanoF'). Data was normalized using Ponceau staining as loading control. Mean ± SE, n = 3–6. *($p < 0.05$). **b.** The cellular morphology of differentiating SH-SY5Y cells was depicted by staining the cells' filamentous actin (F-actin) cytoskeleton and nuclei (in red and blue, respectively). Cells were cultured for 2 days on PLLA nanofibers, in the presence of 10 µM retinoic acid (RA) to induce their neuronal differentiation. Arrows indicate cellular neurite-like projections. Scale bar: 50 µm. **c.** Schematic representation of a possible mechanism for the effects of PLLA nanofibers on neuronal differentiation. F-actin cytoskeleton is presented in red.

proteome that starts to shift towards a morphological and functional state more responsive to differentiation [21,58]. Accordingly, the proteomic data above indicates that these cells have already initiated some of the differentiating events induced by morphogens as RA, such as signaling for hindering cell division and the induction of cytoskeleton remodeling [21].

4. Conclusion

PLLA-based materials have been studied as promising tools for regenerative medicine approaches. Nanofibrous scaffolds have been particularly explored due to their topographical cues that resemble the natural ECM. In this study, we have further explored the cellular responses induced by the interaction between PLLA-based nanofibers and SH-SY5Y cells. Our analyses reveal that PLLA nanofibrous platforms induce a reorganization of the SH-SY5Y cells proteome and differentially activate and inhibit specific cellular functions and signaling pathways. These include blocking cellular proliferation and facilitating cells morphological remodeling and adaptation to the substrate, rendering cells in a more responsive state what ultimately facilitates the onset of cellular differentiation. This knowledge of the cellular behavior on biomaterials is of key importance for the development and optimization of scaffolds that potentiate the regeneration of injured tissues. In the light of the piezoelectric character of PLLA, our group is currently focused on exploiting electrically-induced PLLA polarization and piezoelectricity to deliver further optimized neuritogenic scaffolds.

Acknowledgements

This work was supported by Fundação para a Ciência e a Tecnologia (FCT), Fundo Europeu de Desenvolvimento Regional Portugal (FEDER), QREN-COMPETE Portugal: project PTDC/SAU-NMC/111980/2009, scholarship FRH/BD/47331/2008, Institute for Biomedicine iBiMED UID/BIM/04501/2013, Centre for Cell Biology CBC Pest-OE/SAU/UI0482/2014, Associate Laboratory CICECO (PEst-C/CTM/LA0011/2013), QOPNA research unit (PEst-C/QUI/UI0062/2013), and RNEM (Portuguese Mass Spectrometry Network).

Conflict of Interest

All authors declare no conflicts of interest in this paper

References

1. Seil JT, Webster TJ (2010) Electrically active nanomaterials as improved neural tissue regeneration scaffolds. *Wiley Interdiscip Rev Nanomed Nanobiotechnol* 2: 635-647.
2. Quan Q, Chang B, Meng HY, et al. (2016) Use of electrospinning to construct biomaterials for peripheral nerve regeneration. *Rev Neurosci.*27: 761-768
3. Tian L, Prabhakaran MP, Ramakrishna S (2015) Strategies for regeneration of components of nervous system: scaffolds, cells and biomolecules. *Regen Biomater* 2: 31-45.
4. Yang F, Murugan R, Wang S, et al. (2005) Electrospinning of nano/micro scale poly(L-lactic acid) aligned fibers and their potential in neural tissue engineering. *Biomaterials* 26: 2603-2610.

5. Wang HB, Mullins ME, Cregg JM, et al. (2009) Creation of highly aligned electrospun poly-L-lactic acid fibers for nerve regeneration applications. *J Neural Eng* 6: 016001.
6. Morelli S, Salerno S, Piscioneri A, et al. (2010) Influence of micro-patterned PLLA membranes on outgrowth and orientation of hippocampal neurites. *Biomaterials* 31: 7000-7011.
7. Callahan LA, Xie S, Barker IA, et al. (2013) Directed differentiation and neurite extension of mouse embryonic stem cell on aligned poly(lactide) nanofibers functionalized with YIGSR peptide. *Biomaterials* 34: 9089-9095.
8. Borgens RB (1999) Electrically mediated regeneration and guidance of adult mammalian spinal axons into polymeric channels. *Neuroscience* 91: 251-264.
9. Ding Y, Yan Q, Ruan JW, et al. (2009) Electro-acupuncture promotes survival, differentiation of the bone marrow mesenchymal stem cells as well as functional recovery in the spinal cord-transected rats. *BMC Neurosci* 10: 35.
10. Guo B, Finne-Wistrand A, Albertsson AC (2010) Molecular architecture of electroactive and biodegradable copolymers composed of polylactide and carboxyl-capped aniline trimer. *Biomacromolecules* 11: 855-863.
11. Yang F, Murugan R, Ramakrishna S, et al. (2004) Fabrication of nano-structured porous PLLA scaffold intended for nerve tissue engineering. *Biomaterials* 25: 1891-1900.
12. Yang IH, Co CC, Ho CC (2011) Controlling neurite outgrowth with patterned substrates. *J Biomed Mater Res A* 97: 451-456.
13. Lee YS, Collins G, Arinzeh TL (2011) Neurite extension of primary neurons on electrospun piezoelectric scaffolds. *Acta Biomater* 7: 3877-3886.
14. Lee YS, Arinzeh TL (2012) The influence of piezoelectric scaffolds on neural differentiation of human neural stem/progenitor cells. *Tissue Eng Part A* 18: 2063-2072.
15. He L, Liao S, Quan D, Ma K, et al. (2010) Synergistic effects of electrospun PLLA fiber dimension and pattern on neonatal mouse cerebellum C17.2 stem cells. *Acta Biomaterialia* 6: 2960-2969.
16. Fukada E (2000) History and recent progress in piezoelectric polymers. *IEEE Trans Ultrason Ferroelectr Freq Control* 47: 1277-1290.
17. Corey JM, Gertz CC, Wang BS, et al. (2008) The design of electrospun PLLA nanofiber scaffolds compatible with serum-free growth of primary motor and sensory neurons. *Acta Biomater* 4: 863-8675.
18. He L, Liao S, Quan D, et al. (2010) Synergistic effects of electrospun PLLA fiber dimension and pattern on neonatal mouse cerebellum C17.2 stem cells. *Acta Biomater* 6: 2960-2969.
19. Evans GR, Brandt K, Widmer MS, et al. (1999) In vivo evaluation of poly(L-lactic acid) porous conduits for peripheral nerve regeneration. *Biomaterials* 20: 1109-1115.
20. Yu Y, Meng D, Man L, et al. (2016) The Interactions Between Aligned Poly(L-Lactic Acid) Nanofibers and SH-SY5Y Cells In Vitro. *J Nanosci Nanotechnol* 16: 6407-6413.
21. da Rocha JF, da Cruz e Silva OA, Vieira SI (2015) Analysis of the amyloid precursor protein role in neuritogenesis reveals a biphasic SH-SY5Y neuronal cell differentiation model. *J Neurochem* 134: 288-301.
22. Koh HS, Yong T, Chan CK, et al. (2008) Enhancement of neurite outgrowth using nano-structured scaffolds coupled with laminin. *Biomaterials* 29: 3574-3582.
23. Pina S, Vieira SI, Rego P, et al. (2010) Biological responses of brushite-forming Zn- and ZnSr-substituted beta-tricalcium phosphate bone cements. *Eur Cell Mater* 20: 162-177.

24. Ishihama Y, Oda Y, Tabata T, et al. (2005) Exponentially modified protein abundance index (emPAI) for estimation of absolute protein amount in proteomics by the number of sequenced peptides per protein. *Mol Cell Proteomics* 4: 1265-1272.
25. Mi H, Thomas P (2009) PANTHER pathway: an ontology-based pathway database coupled with data analysis tools. *Methods Mol Biol* 563: 123-140.
26. Milacic M, Haw R, Rothfels K, et al. (2012) Annotating cancer variants and anti-cancer therapeutics in reactome. *Cancers (Basel)* 4: 1180-1211.
27. Fabregat A, Sidiropoulos K, Garapati P, et al. (2016) The Reactome pathway Knowledgebase. *Nucleic Acids Res* 44: D481-D487.
28. Henriques AG, Vieira SI, Crespo-López ME, et al. (2009) Intracellular sAPP retention in response to Abeta is mapped to cytoskeleton-associated structures. *J Neurosci Res* 87: 1449-1461.
29. Romero-Calvo I, Ocón B, Martínez-Moya P, et al. (2010) Reversible Ponceau staining as a loading control alternative to actin in Western blots. *Anal Biochem* 401: 318-320.
30. Nistor G, Poole AJ, Draelos Z, et al. (2016) Human Stem Cell-Derived Skin Progenitors Produce Alpha 2-HS Glycoprotein (Fetuin): A Revolutionary Cosmetic Ingredient. *J Drugs Dermatol* 15: 583-598.
31. Elsas J, Sellhaus B, Herrmann M, et al. (2013) Fetuin-a in the developing brain. *Dev Neurobiol* 73: 354-369.
32. Werbowetski-Ogilvie TE, Agar NY, Waldkircher de Oliveira RM, et al. (2006) Isolation of a natural inhibitor of human malignant glial cell invasion: inter alpha-trypsin inhibitor heavy chain 2. *Cancer Res* 66: 1464-1472.
33. Ono S (2007) Mechanism of depolymerization and severing of actin filaments and its significance in cytoskeletal dynamics. *Int Rev Cytol* 258: 1-82.
34. Shekhar S, Pernier J, Carlier MF (2016) Regulators of actin filament barbed ends at a glance. *J Cell Sci* 129: 1085-1091.
35. Barlat I, Maurier F, Duchesne M, et al. (1997) A role for Sam68 in cell cycle progression antagonized by a spliced variant within the KH domain. *J Biol Chem* 272: 3129-3132.
36. Tsuji T, Ficarro SB, Jiang W (2006) Essential role of phosphorylation of MCM2 by Cdc7/Dbf4 in the initiation of DNA replication in mammalian cells. *Mol Biol Cell* 17: 4459-4472.
37. De Vos WH, Houben F, Hoebe RA, et al. (2010) Increased plasticity of the nuclear envelope and hypermobility of telomeres due to the loss of A-type lamins. *Biochim Biophys Acta* 1800: 448-458.
38. Nardella M, Guglielmi L, Musa C, et al. (2015) Down-regulation of the Lamin A/C in neuroblastoma triggers the expansion of tumor initiating cells. *Oncotarget* 6: 32821-32840.
39. Jurica MS, Licklider LJ, Gygi SR, et al. (2002) Purification and characterization of native spliceosomes suitable for three-dimensional structural analysis. *RNA* 8: 426-439.
40. Weidensdorfer D, Stöhr N, Baude A, et al. (2009) Control of c-myc mRNA stability by IGF2BP1-associated cytoplasmic RNPs. *RNA* 15: 104-115.
41. Nami B, Ghasemi-Dizgah A, Vaseghi A (2016) Overexpression of molecular chaperons GRP78 and GRP94 in CD44(hi)/CD24(lo) breast cancer stem cells. *Bioimpacts* 6: 105-110.
42. Zhou H, Zhang Y, Fu Y, et al. (2011) Novel mechanism of anti-apoptotic function of 78-kDa glucose-regulated protein (GRP78): endocrine resistance factor in breast cancer, through release of B-cell lymphoma 2 (BCL-2) from BCL-2-interacting killer (BIK). *J Biol Chem* 286: 25687-25696.

43. Boulares AH, Yakovlev AG, Ivanova V, et al. (1999) Role of poly(ADP-ribose) polymerase (PARP) cleavage in apoptosis: Caspase 3-resistant PARP mutant increases rates of apoptosis in transfected cells. *J Biol Chem* 274: 22932-22940.
44. Ahel I, Ahel D, Matsusaka T, et al. (2008) Poly(ADP-ribose)-binding zinc finger motifs in DNA repair/checkpoint proteins. *Nature* 451: 81-85.
45. Moosmann P, Georgiev O, Le Douarin B, et al. (1996) Transcriptional repression by RING finger protein TIF1 beta that interacts with the KRAB repressor domain of KOX1. *Nucleic Acids Res* 24: 4859-48567.
46. Riclet R, Chendeb M, Vonesch JL, et al. (2009) Disruption of the interaction between transcriptional intermediary factor 1{beta} and heterochromatin protein 1 leads to a switch from DNA hyper- to hypomethylation and H3K9 to H3K27 trimethylation on the MEST promoter correlating with gene reactivation. *Mol Biol Cell* 20: 296-305.
47. Shim KS, Lubec G. Drebrin, a dendritic spine protein, is manifold decreased in brains of patients with Alzheimer's disease and Down syndrome. *Neurosci Lett* 324: 209-212.
48. Ponuwei GA (2016) A glimpse of the ERM proteins. *J Biomed Sci* 23: 35.
49. Liu CX, Xu X, Chen XL, et al. (2015) Glutamate promotes neural stem cell proliferation by increasing the expression of vascular endothelial growth factor of astrocytes in vitro. *Cell Mol Biol* 61: 75-84.
50. Semrad TJ, Mack PC (2012) Fibroblast growth factor signaling in non-small-cell lung cancer. *Clin Lung Cancer* 13: 90-95.
51. Yano S, Kondo K, Yamaguchi M, et al. (2003) Distribution and function of EGFR in human tissue and the effect of EGFR tyrosine kinase inhibition. *Anticancer Res* 23: 3639-3650.
52. Mizuguchi Y, Specht S, Isse K, et al. (2015) Breast tumor kinase/protein tyrosine kinase 6 (Brk/PTK6) activity in normal and neoplastic biliary epithelia. *J Hepatol* 63: 399-407.
53. Lee S, Suh GY, Ryter SW, et al. (2016) Regulation and Function of the Nucleotide Binding Domain Leucine-Rich Repeat-Containing Receptor, Pyrin Domain-Containing-3 Inflammasome in Lung Disease. *Am J Respir Cell Mol Biol* 54: 151-160.
54. Goshima Y, Yamashita N, Nakamura F, et al. (2016) Regulation of dendritic development by Semaphorin 3A through novel intracellular remote signaling. *Cell Adh Migr* 8: 1-14.
55. Mo XM, Xu CY, Kotaki M, et al. (2004) Electrospun P(LLA-CL) nanofiber: a biomimetic extracellular matrix for smooth muscle cell and endothelial cell proliferation. *Biomaterials* 25: 1883-1890.
56. da Silva JS, Dotti CG (2002) Breaking the neuronal sphere: regulation of the actin cytoskeleton in neuritogenesis. *Nat Rev Neurosci* 3: 694-704.
57. Siegel G, Agranoff B, Albers R, et al. (1999) Basic Neurochemistry: Molecular, Cellular and Medical Aspects 6 ed. Philadelphia: Lippincott-Raven.
58. Estefanía MM, Ganier O, Hernández P, et al. (2012) DNA replication fading as proliferating cells advance in their commitment to terminal differentiation. *Sci Rep* 2: 279.
59. Tzoneva R, Faucheux N, Groth T (2007) Wettability of substrata controls cell-substrate and cell-cell adhesions. *Biochim Biophys Acta* 1770: 1538-1547.
60. Alves NM, Shi J, Oramas E, et al. (2009) Bioinspired superhydrophobic poly(L-lactic acid) surfaces control bone marrow derived cells adhesion and proliferation. *J Biomed Mater Res A* 91: 480-488.
61. Titushkin I, Cho M (2009) Regulation of cell cytoskeleton and membrane mechanics by electric field: role of linker proteins. *Biophys J* 96: 717-728.

62. Wen X, Tresco PA (2006) Effect of filament diameter and extracellular matrix molecule precoating on neurite outgrowth and Schwann cell behavior on multifilament entubulation bridging device in vitro. *J Biomed Mater Res A* 76: 626-637.
63. Weitzdoerfer R, Fountoulakis M, Lubec G (2001) Aberrant expression of dihydropyrimidinase related proteins-2,-3 and -4 in fetal Down syndrome brain. *J Neural Transm Suppl* 61: 95-107.

Supplementary

Table S1. Identity of the 45 proteins identified by MS/MS with different expression on Control and NanoF samples.

Proteins Upregulated in NanoF		Proteins Downregulated in NanoF	
Unique in NanoF	UpR in NanoF	Unique in Control	DownR in NanoF
Alpha-2-macroglobulin	Serum albumin	Aminopeptidase B	ATP-citrate synthase
Complement C3	Alpha-fetoprotein	Cytoskeleton-associated	Probable ATP-dependent RNA helicase
Hemoglobin subunit	Alpha-2-HS-glyc	protein 4	DDX5
alpha	oprotein	Cytoplasmic dynein 1	Drebrin
Hemoglobin subunit	Gelsolin	intermediate chain 2	Dihydropyrimidinase-related protein 3
beta	Inter-alpha-trypsi	Dipeptidyl peptidase 3	78 kDa glucose-regulated protein
Inter-alpha-trypsin	n inhibitor heavy	Dihydropyrimidinase-related	Heat shock protein HSP 90-alpha
inhibitor heavy chain	chain H2	protein 2	Heat shock protein HSP 90-beta
H4	Septin-9	Neutral alpha-glucosidase AB	Heat shock 70 kDa protein 1A/1B
DNA repair and		Ras GTPase-activating	Heat shock cognate 71 kDa protein
recombination protein		protein-binding protein 2	Interleukin enhancer-binding factor 3
RAD54-like		Kinesin-1 heavy chain	Mitochondrial inner membrane protein
		DNA replication licensing	Prelamin-A/C
		factor MCM7	Poly [ADP-ribose] polymerase 1
		Nuclear pore complex protein	Heterogeneous nuclear
		Nup93	ribonucleoprotein U
		U4/U6 small nuclear	Heterogeneous nuclear
		ribonucleoprotein Prp3	ribonucleoprotein M
		Splicing factor 3A subunit 1	KH domain-containing, RNA-binding,
		116 kDa U5 small nuclear	signal transduction-associated protein 1
		ribonucleoprotein component	DNA replication licensing factor
			MCM5
			Radixin
			Lysosome membrane protein 2
			Transcription intermediary factor 1-beta